Applied Surface Science 492 (2019) 239–244

Contents lists available at ScienceDirect

Applied Surface Science

journal homepage: www.elsevier.com/locate/apsusc

Full length article

Nucleation engineering for atomic layer deposition of uniform sub-10 nm high-K dielectrics on $MoTe_2$

Yu-Shu Lin[a], Iljo Kwak[b], Tsai-Fu Chung[a], Jer-Ren Yang[a], Andrew C. Kummel[b], Miin-Jang Chen[a,*]

[a] Department of Materials Science and Engineering, National Taiwan University, Taipei 10617, Taiwan
[b] Department of Chemistry and Biochemistry, University of California, San Diego, CA 92093, United States

ARTICLE INFO

Keywords:
Two-dimensional materials
Transition metal dichalcogenides (TMDs)
Atomic layer deposition (ALD)
High-K dielectrics

ABSTRACT

Continuous, uniform, and sub-10 nm Al_2O_3 high-K dielectrics upon two-dimensional exfoliated multilayer $MoTe_2$ are realized by atomic layer deposition (ALD) based on a nucleation layer (NL) prepared by the ozone-based process, interfacial AlN, and low-temperature (low-*T*) physical adsorption. The NLs gives rise to significant reduction of the leakage current in the sub-10 nm Al_2O_3 high-K dielectrics as shown by conductive atomic force microscopy. For the ozone-based NL, X-ray photoelectron spectroscopy (XPS) reveals the oxidation of $MoTe_2$ which is detrimental to the electrical properties of $MoTe_2$. For the AlN NL, XPS reveals that Mo—N bonds were formed without Mo—O bonds and no chemical shift appeared in Te-*3d* XPS spectrum, indicating the AlN NL did not result in the $MoTe_2$ oxidation but instead the formation of an MoN layer. For the low-*T* NL, the XPS spectra of $MoTe_2$ are the same as those of the as-exfoliated $MoTe_2$ flake, consistent with the absence of chemical reactions during low-*T* physical adsorption. The result demonstrates that the NLs prepared by the low-*T* physical adsorption and the interfacial AlN are effective and favorable for nucleating high-quality high-K gate dielectrics on $MoTe_2$ transistors.

1. Introduction

Owing to the atomic thickness and suitable bandgap of two-dimensional transition metal dichalcogenides (TMDs) [1], TMDs have been widely explored as promising candidates for channel materials as the scaling of Si field-effect transistors approaches the physical limit [2–8]. The chemical formula of TMDs is MX_2, where M represents a transition metal including Mo, W, and Hf, and X is a chalcogen element such as S, Se, or Te. Among numerous TMDs, molybdenum ditelluride (α-$MoTe_2$) is worthy of attention because of its attractive properties. Bandgap energies of monolayer and bulk $MoTe_2$ are 1.10 eV (direct) and 0.85–1.0 eV (indirect), respectively [9–11]. Density functional theory predicts a high electron mobility for $MoTe_2$ [12]. In addition, the ambipolar conductivity in $MoTe_2$ field effect transistors has been reported [13–17].

The interface quality between high-K dielectrics and semiconductor channels plays an important role in the performance of TMDs transistors. However, it is difficult to deposit high-quality high-K dielectrics on TMDs by atomic layer deposition (ALD) because islands or clusters are usually formed on pristine TMDs due to the lack of dangling bonds [18,19]. In order to overcome the challenges from the chemical inertness of TMDs, investigations have been conducted upon nucleation engineering on TMD surfaces [20–24]. For example, continuous high-K dielectrics prepared by ozone-based ALD have been achieved without detectable oxidation states on MoS_2 [22]. The "NanoFog ALD" technique also produces a uniform layer of high-quality Al_2O_3 on 2D materials without surface chemical reactions based on low-temperature (low-*T*) physical adsorption [24–26]. An AlN nucleation layer (NL) has been proposed to realize uniform deposition of high-quality Al_2O_3 on MoS_2, and the electrical stability of TMDs transistors was greatly improved as a result of the low border trap density [27]. Although these techniques work well on MoS_2 surfaces, extension of these methods to other TMDs may be challenges because of the difference in surface properties. For example, as compared with MoS_2, selenium-based TMDs suffer from surface oxidation during the oxygen functionalization due to the favorable oxidation thermochemistry [28].

In this paper, the nucleation engineering for ALD of high-quality high-K dielectrics on exfoliated $MoTe_2$ is investigated using the ozone-based process, the low-*T* physical adsorption, and the interfacial AlN deposition. An ultrathin NL was prepared to provide nucleation sites for the subsequent deposition of an high-K layer, as shown schematically in Fig. 1. X-ray photoelectron spectroscopy (XPS) and conductive atomic force microscopy (CAFM) were used to characterize the chemical states and the leakage current of high-K dielectrics on $MoTe_2$. Continuous and

* Corresponding author.
E-mail address: mjchen@ntu.edu.tw (M.-J. Chen).

https://doi.org/10.1016/j.apsusc.2019.06.192
Received 19 March 2019; Received in revised form 31 May 2019; Accepted 19 June 2019
Available online 20 June 2019
0169-4332/

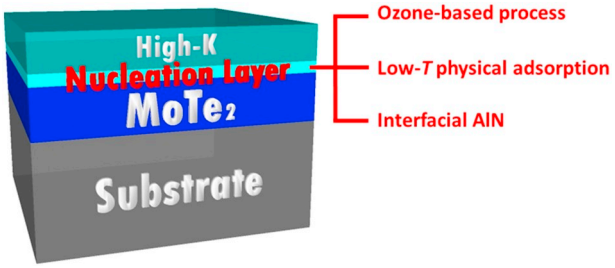

Fig. 1. Schematic diagram of the high-K dielectric stacks on $MoTe_2$. The nucleation layer (NL) was prepared by the ozone-based process, low-temperature (low-*T*) physical adsorption, and interfacial AlN, respectively.

uniform Al_2O_3 high-K dielectrics can be deposited on $MoTe_2$ with the NL prepared by the three techniques. However, the ozone-based process results in the oxidation of $MoTe_2$, which will degrade the electrical performance of $MoTe_2$. No noticeable oxidization was observed with the NL formed by the low-*T* physical adsorption or interfacial AlN, indicating the high-quality nucleation engineering for ALD of continuous, uniform, low-leakage, and sub-10 nm high-K dielectrics on $MoTe_2$.

2. Experimental

The layer structure of high-K dielectric stacks is depicted schematically in Fig. 1. First, multilayer $MoTe_2$ flakes were transferred onto a *p*-type Si (100) wafer from 2H-$MoTe_2$ (HQ Graphene) single crystal using mechanical exfoliation with Nitto tape. Trimethylaluminum (TMA) and ozone were used as the precursors for the ozone-based NL. Because a low temperature of 80 °C was suggested in the ozone-based ALD process to prepare a NL for a continuous and thin Al_2O_3 layer on MoS_2 [22], the deposition of ozone-based Al_2O_3 NL was conducted at 80 °C with 10 ALD cycles in this work. For the deposition of the Al_2O_3 NL using low-*T* physical adsorption, the precursors were TMA and H_2O vapor. The H_2O-based Al_2O_3 NL was prepared at 80 °C with 20 ALD cycles along with a short purge time to achieve physical adsorption of the NL [24]. For the deposition of interfacial AlN, TMA and remote N_2/H_2 plasma were used to deposit the AlN NL at 200 °C with 10 ALD cycles [29]. Remote nitrogen ions/radicals were generated by a radio-frequency coil at a low power of 50 W. Afterwards, an Al_2O_3 main dielectric layer was prepared with 40 ALD cycles upon the NL using TMA and H_2O vapor as aluminum and oxygen sources at 200 °C. The details of ALD recipes have been provided in Table 1.

Surface morphologies of the Al_2O_3 main layers were measured by tapping-mode atomic force microscopy (AFM, Bruker Dimension Icon). CAFM (Bruker D3100) with a $PtIr_5$-coated Si tip was used to probe the leakage current through the Al_2O_3 dielectrics on $MoTe_2$. The thickness of high-K dielectric stacks was examined by high-resolution transmission electron microscopy (HRTEM, FEI Tecnai G2 F20). The binding energy of MoS_2 flakes was characterized by *ex-situ* XPS (Thermo Fisher Scientific Theta Probe) with an Al Kα X-ray source (1486.6 eV) and a spot size of 400 μm in diameter.

Results and discussion

Fig. 2(a) shows the AFM image and 3D topography of the Al_2O_3 main layer (100 ALD cycles) which was directly deposited on $MoTe_2$ at 200 °C without any NL (Fig. 2(a′)). It is seen that the nucleation proceeds in a sporadic manner, giving rise to a rough and discontinuous surface. The result can be attributed to weak adhesion of TMA and H_2O on the chemical inertness surface of TMDs [22,28]. In order to deposit a continuous high-K dielectric layer on $MoTe_2$, NLs were introduced between the Al_2O_3 main layer and $MoTe_2$ using the ozone-based process, the low-*T* physical adsorption, and the interfacial AlN deposition. Figs. 2(b), (c), and (d) show AFM images and 3D topographies of the Al_2O_3 main layers, and the corresponding layer structures are depicted in Figs. 2(b′), (c′) and (d′). In contrast to Fig. 2(a), continuous and uniform surfaces of the Al_2O_3 main layers were observed in Fig. 2(b)~(d). Because ozone is easily decomposed into molecular O_2 and active O radicals in the ozone-based process, the reaction of ozone with TMDs surfaces provides nucleation sites on the dangling-bond free surfaces [22,30]. Hence the ozone-based process improves the coverage and uniformity of the Al_2O_3 layer on the $MoTe_2$ basal plane. On the other hand, the low-*T* physical adsorption technique, which relies on a low deposition temperature below 100 °C and a short purge time between the precursor and reactant pulses, is also known as the "NanoFog ALD" method [25,26]. At low deposition temperatures, the thermal energy of precursors/reactants is lower than the potential well depth of physical adsorption. Thus the precursors/reactants might be trapped in the adsorption potential well [20,22,31,32]. As a result, the excess precursors/reactants are physisorbed on the $MoTe_2$ surface at a deposition temperature at 80 °C. The physisorbed precursors/reactants do not have enough time to desorb from the $MoTe_2$ surface if the purge time between the TMA and H_2O pulses is short, resulting in the deposition of a Al_2O_3 NL. This Al_2O_3 NL offers nucleation sites for subsequent deposition of the high-K main layer at a higher temperature. For the interfacial AlN method, the uniform deposition of the continuous AlN/Al_2O_3 dielectric stack on $MoTe_2$ may result from the preferential removal of tellurium (Te), which provides dangling bonds to form the nucleation sites. The detail is revealed in the XPS characterization in the later section.

Fig. 3 shows cross-sectional HRTEM images of the high-K dielectric stacks, in which the NLs were prepared by the ozone-based process, the low-*T* physical adsorption, and the interfacial AlN deposition. It can be seen that the total thickness (d_{total}) of the high-K dielectric stacks is ~5.9, 9.4 and 5.2 nm, respectively, and the thickness (d_{NL}) is about 1.8 and 1.1 nm for the NLs prepared by the ozone-based process and the interfacial AlN deposition. Thus the thickness of the Al_2O_3 main layer (d_{main}) is ~4.1 nm, which can be deduced from Fig. 3(a) and (c). Accordingly, the thickness of the NL (d_{NL}) prepared by the low-*T* physical adsorption can be estimated to be ~5.3 nm, even though the interface between the NL and the Al_2O_3 main layer is not obvious in the TEM image (Fig. 3(b)) since the Al_2O_3 in both layers was prepared with the same H_2O-based process. Such a thick NL is attributed to precursor condensation on the $MoTe_2$ surface at a low deposition temperature along with a short purge time. Notice that an interface between the NL and $MoTe_2$ can be observed in Fig. 3(a) and the $MoTe_2$ lattice fringes

Table 1
The details of ALD recipes. The longer TMA and H_2O pulse times and the short purge times in the low-*T* physical adsorption process were used to achieve physical adsorption of the NL.

Method	TMA pulse time	TMA purge time	Reactant pulse time	Reactant purge time	Deposition temperature
Ozone-based process	0.02 s	15 s	0.02 s (ozone)	15 s	80 °C
Low-*T* physical adsorption	0.2 s	1 s	0.2 s (H_2O)	1 s	80 °C
Interfacial AlN	0.02 s	15 s	55 s (N_2/H_2 plasma)	15 s	200 °C
Al_2O_3 main layer	0.02 s	15 s	0.02 s (H_2O)	15 s	200 °C

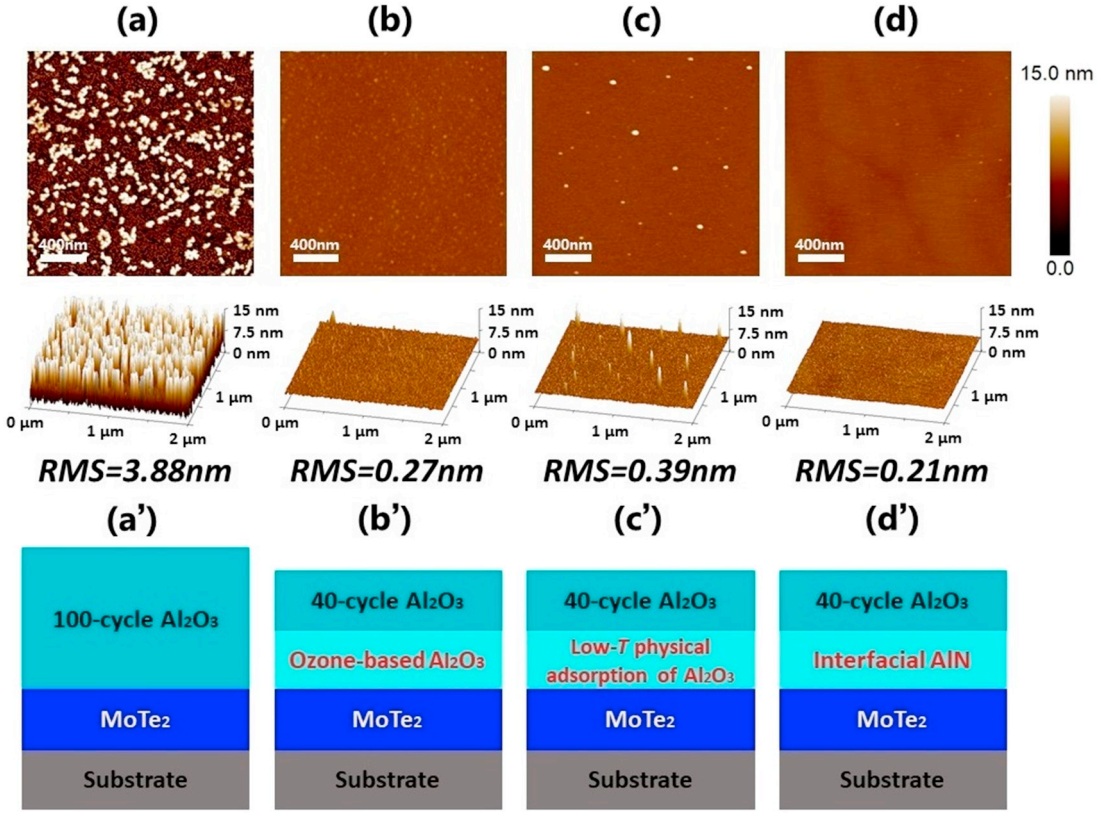

Fig. 2. AFM images and 3D topographies (a)–(d) of the Al_2O_3 high-K dielectrics on $MoTe_2$ along with the root mean square (RMS) roughness and the corresponding layer structure (a′)–(d′). Each AFM image is $2 \times 2\,\mu m^2$ in area with a scale bar of 400 nm. As compared with the AFM 3D topographies shown in (b) (with the ozone-based NL) and (d) (with the AlN NL), the presence of nanoscale particles in (c), which is known as the so-called "NanoFog", is attributed to the incomplete removal (purge away) of precursor/reactant as a result of the short purge time at a low deposition temperature. The result demonstrates that the continuous and uniform Al_2O_3 high-K dielectrics with a thickness below 10 nm can be achieved on $MoTe_2$ with the NLs.

are seen near the interface. Therefore, the layer underneath the NL might be a damaged $MoTe_2$ region with a thickness of ~1.1 nm, resulting from high reactivity of the ozone-based process. The TEM images clearly demonstrate that continuous and uniform Al_2O_3 high-K dielectrics with a thickness below 10 nm can be achieved on $MoTe_2$ with the NLs prepared by the ozone-based process, the low-*T* physical adsorption, and the interfacial AlN deposition.

The CAFM measurement is illustrated schematically in Fig. 4, where a DC bias was applied to the *p*-type Si substrate and the AFM tip was scanned in the contact mode over the Al_2O_3 surface. Fig. 5 displays the mapping and the 3D CAFM topographies (Fig. 5(a)–(d)) of the leakage current through the Al_2O_3 high-K dielectrics on $MoTe_2$, and the statistical leakage current distributions (Fig. 5(a′)–(d′)), respectively, with the corresponding layer structure of each dielectric stack shown in Fig. 2(a′)–(d′). Fig. 5(a) shows that a large leakage current is present if Al_2O_3 was deposited directly on $MoTe_2$ at 200 °C without any NL, which is attributed to the island structure as shown in Fig. 2(a). The introduction of the NL between the Al_2O_3 main layer and $MoTe_2$ gives rise to a very low leakage current close to the noise level of CAFM, as shown in Fig. 5(b)–(d). The outcome clearly indicates that the continuous and uniform Al_2O_3 high-K dielectrics lead to a low leakage current as a result of the NLs prepared by the ozone-based process, the low-*T* physical adsorption, and the interfacial AlN deposition.

Because the chemical shift reveals the change in binding energies,

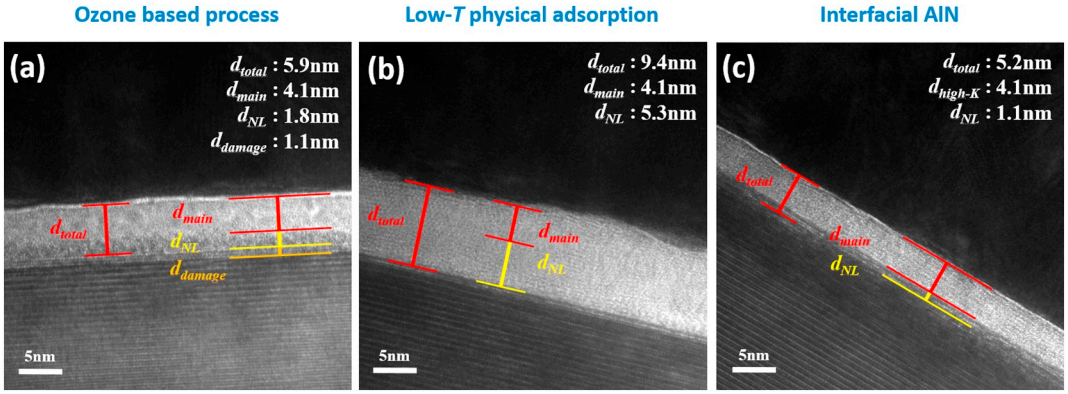

Fig. 3. Cross-sectional HRTEM images of the high-K dielectric stacks with the NL prepared by (a) the ozone-based process, (b) the low-*T* physical adsorption, and (c) the interfacial AlN deposition.

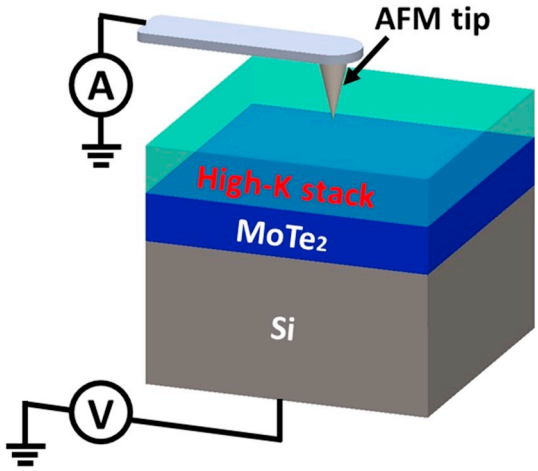

Fig. 4. Schematic diagram of the CAFM measurement of the high-K dielectric stacks on $MoTe_2$.

XPS has been extensively used for the interface characterization of TMDs. Fig. 6(a) and (b) show the Mo-*3d* and Te-*3d* XPS spectra of the as-exfoliated multilayer $MoTe_2$ and that covered with the high-K dielectric stack, respectively. As compared with the XPS spectra of the as-exfoliated $MoTe_2$, the NL prepared by the ozone-based process yields additional Mo-*3d* and Te-*3d* peaks at higher binding energies, which correspond to the Mo^{6+} (MoO_3) and Te^{4+} (TeO_2) states, respectively. The formation of MoO_3 and TeO_2 provides the nucleation sites for subsequent deposition of the continuous and uniform high-K layer [20,33]. However, MoO_3 and TeO_2 have wide bandgaps of ~3.1 eV [34] and ~3.3 eV [35], respectively, which are much higher than that of $MoTe_2$ [36]. Therefore, the electrical properties of $MoTe_2$ would be degraded by the $MoTe_2$ oxidation due to the band discontinuity [21]. Therefore, a NL formation process is required which prevents the oxidation of $MoTe_2$ during the ALD process. Please notice that the ozone-based ALD process does not result in the oxidation of MoS_2 [22], consistent with the high reactivity of $MoTe_2$ to oxidants. In contrast, the Mo-*3d* and Te-*3d* XPS spectra of the sample with the low-*T* physical adsorption NL is almost identical to those of the as-exfoliated $MoTe_2$. The XPS data is consistent with the absence of chemical reactions if the deposition of NL proceeds through the physical adsorption; therefore, the oxidation of molybdenum and telluride can be avoided by using the physical adsorption at low temperatures [37,38]. In the $MoTe_2$ sample with the AlN interfacial layer, the Mo—N peak is observed in the Mo-*3d* XPS spectrum, which is ~0.4 eV higher than the Mo—Te peak due to hybridization of the Mo-*3d* and N-*2p* orbitals [39–41]. In contrast to the Mo—O bond which is detrimental to the electrical characteristics of $MoTe_2$, previous studies have indicated that the Mo—N bonding does not cause the degradation of the electrical properties of Mo-based TMDs [27,39].

Table 2 lists the atomic ratio of Te to Mo ($MoTe_x$) of the as-exfoliated multilayer $MoTe_2$ and that covered with the high-K dielectric stack, which were obtained from the analysis of XPS spectra shown in Fig. 6. The tellurium content in $MoTe_x$ decreases significantly if the NLs are deposited by the ozone-based process and the interfacial AlN deposition, suggesting that tellurium might be removed by oxygen and nitrogen. Note that the tellurium content of the sample with the NL prepared by the low-*T* physical adsorption is the same as that of the as-exfoliated $MoTe_2$. The result is consistent with the inference from the XPS spectra, revealing the lack of chemical reactions at the $MoTe_2$ surface as the NL is deposited by the low-*T* physical adsorption.

Since Raman spectroscopy is a versatile tool to characterize TMDs structures [42–44], Raman spectra were measured for the as-exfoliated $MoTe_2$ and that covered with the NLs prepared by the ozone-based process, the low-*T* physical adsorption, and the interfacial AlN deposition, respectively (Fig. 7). The Raman peaks at ~235 cm^{-1} and ~174 cm^{-1} are associated with the $E_{2g}{}^1$ and A_{1g} modes of bulk $MoTe_2$ [45]. As compared with exfoliated $MoTe_2$, no detectable variation in

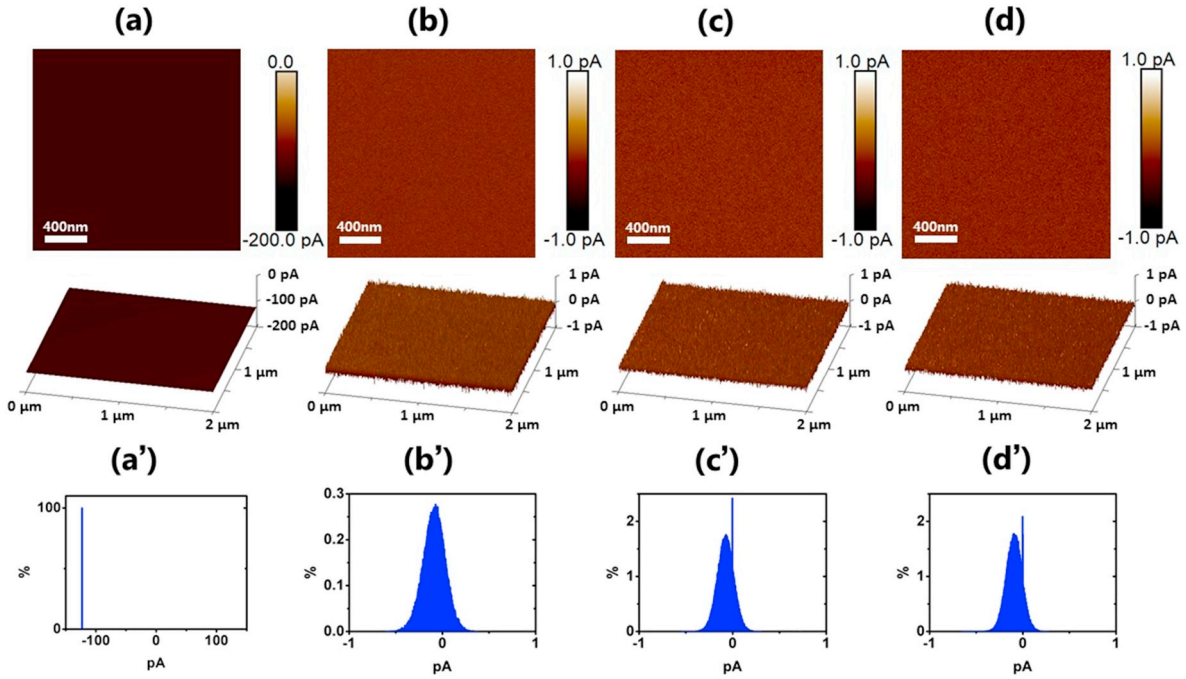

Fig. 5. The CAFM leakage current maps and the 3D CAFM topographies (a)–(d), and the statistical leakage current distributions (a′)–(d′), of the Al_2O_3 high-K dielectrics with the corresponding layer structure shown in Figs. 2 (a′)–(d′). The applied DC bias was −3 V across the high-K dielectric stacks. Each CAFM image is $2 \times 2\,\mu m^2$ in area with a scale bar of 400 nm. As shown in (a) and (a′), all the data points are ~122 pA (the upper limit for instrument protection) since the leakage current is higher than the upper limit set by the CAFM measurement, which is attributed to the island structure as shown in Fig. 2(a).(b)–(d) and (b′)–(d′) show that the leakage current is very low (close to the noise level of CAFM) as a result of the formation of continuous and uniform Al_2O_3 high-K dielectrics. The result shows that the leakage current decreases significantly with the introduction of the NLs.

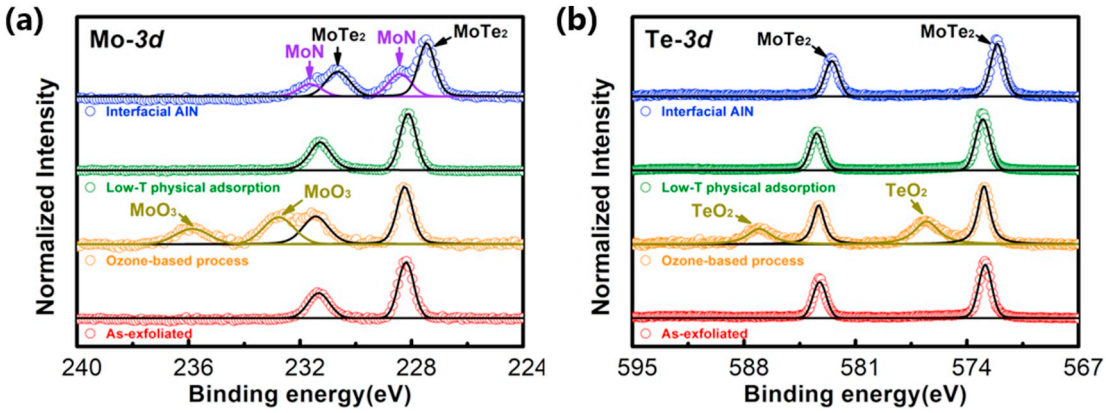

Fig. 6. XPS spectra of the (a) Mo *3d*, and (b) Te *3d* core levels of the as-exfoliated $MoTe_2$ (red) and that covered with the high-K dielectric stack, in which the NL was prepared by the ozone-based process (orange), low-T physical adsorption (green), and interfacial AlN (blue). (For interpretation of the references to color in this figure legend, the reader is referred to the web version of this article.)

Table 2
Stoichiometry of as-exfoliated $MoTe_2$ and that covered with the high-K dielectric stack, in which the NLs were prepared by the ozone-based process, interfacial AlN, and low-*T* physical adsorption.

$MoTe_x$ sample	x valve
As-exfoliated $MoTe_2$	1.9
NL prepared by ozone-based process	1.3
NL prepared by interfacial AlN	1
NL prepared by low-*T* physical adsorption	1.9

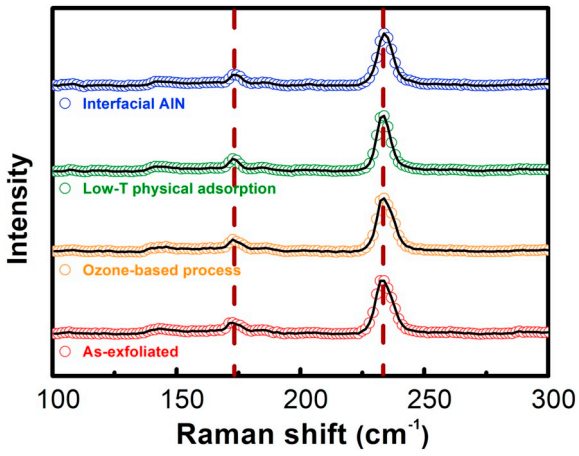

Fig. 7. Raman spectra of the as-exfoliated $MoTe_2$ (red) and that covered with the high-K dielectric stack, in which the NL was prepared by the ozone-based process (orange), low-T physical adsorption (green), and interfacial AlN (blue). (For interpretation of the references to color in this figure legend, the reader is referred to the web version of this article.)

the Raman peaks was observed as the NL was prepared by the low-*T* physical adsorption. It should be noted that even the AlN interfacial and the ozone-based processes, which result in surface oxidation and nitridation as shown in the XPS spectra (Fig. 6), do not give rise to any obvious change in the Raman spectra. This result can be ascribed to the fact that both oxidation and nitridation occur only at the region close to the $MoTe_2$ surface. Because the probed depth of Raman scattering (> ~1000 nm) is much deeper than that of XPS (~5 nm), XPS characterization is more sensitive to the surface oxidation and nitridation than Raman spectroscopy.

A comparison of the low-*T* physical adsorption method, which was performed on $MoTe_2$ and MoS_2, is provided and discussed as follows. Fig. S1 (a)(b) in Supplementary Materials display the AFM images and 3D topographies of the Al_2O_3 main layers together with the corresponding layer structures as schematically illustrated in Figs. S1 (a′)(b′), in which the NLs were prepared with the purge time of 1 and 2 s, respectively, on $MoTe_2$. A decrease of the purge time from 2 to 1 s leads to a dramatic transformation of the Al_2O_3 main layer from a sporadic/pinhole-like structure (with a large RMS roughness of 2.65 nm) to a continuous film (with a low RMS roughness of 0.39 nm). A shorter purge time results in more residues of precursors/reactants on the $MoTe_2$ surface, resulting in more physical adsorption of precursors/reactants. The precursors/reactants adsorbed on the TMD surface provide the nucleation sites for the subsequent Al_2O_3 deposition. Therefore, the shorter purge time, the more residues of precursors/reactants and nucleation sites, which lead to the formation of a continuous Al_2O_3 main layer. Fig. S2 (a)(b) and (a′)(b′) in Supplementary Materials show the AFM images and 3D topographies of the Al_2O_3 main layers and their layer structures on $MoTe_2$ and MoS_2, respectively. For the formation of a continuous Al_2O_3 main layer as shown in Figs. S2 (a) and (b), the required purge time (1 s) for the NL deposited on $MoTe_2$ is shorter than on that on MoS_2 (5 s). If the precursors/reactants are difficult to adsorb on the TMD surface, a shorter purge time is needed to increase the residues of precursors/reactants. Therefore, Fig. S2 suggests that the physical adsorption of precursors/reactants on $MoTe_2$ is more difficult than that on MoS_2. The result indicates that the purge time is a critical processing parameter for the NLs prepared by the low-*T* physical adsorption technique on different 2D materials.

3. Conclusion

Continuous, uniform, low-leakage, and sub-10 nm Al_2O_3 high-K dielectrics on $MoTe_2$ are demonstrated in this study through the nucleation engineering based on the ozone-based process, the low-*T* physical adsorption, and the interfacial AlN deposition. The CAFM measurement demonstrates that the introduction of the NL between the Al_2O_3 main layer and $MoTe_2$ leads to significant reduction of the leakage current. Nevertheless, the oxidation of $MoTe_2$ takes place as the NL was prepared by the ozone-based process, which is unfavorable to the device characteristics of $MoTe_2$. Conversely, the low-*T* physical adsorption and the interfacial AlN deposition do not result in the oxidization of $MoTe_2$ but instead the formation of a weakly interacting interface or a MoN interface, respectively; these two interfaces may be preferable for nucleation engineering of high-quality high-K gate dielectrics on $MoTe_2$ transistors.

Acknowledgment

The authors gratefully acknowledge the financial support from

Taiwan Semiconductor Manufacturing Company (TSMC) and the Ministry of Science and Technology (MOST 107-2622-8-002-018), Taiwan.

Appendix A. Supplementary data

Supplementary data to this article can be found online at https://doi.org/10.1016/j.apsusc.2019.06.192.

References

[1] Q.H. Wang, K. Kalantar-Zadeh, A. Kis, J.N. Coleman, M.S. Strano, Electronics and optoelectronics of two-dimensional transition metal dichalcogenides, Nat. Nanotechnol. 7 (2012) 699–712.

[2] K.S. Novoselov, A.K. Geim, S.V. Morozov, D. Jiang, Y. Zhang, S.V. Dubonos, I.V. Grigorieva, A.A. Firsov, Electric field effect in atomically thin carbon films, Science 306 (2004) 666–669.

[3] A.K. Geim, I.V. Grigorieva, Van der Waals heterostructures, Nature 499 (2013) 419–425.

[4] X. Wang, P. Wang, J. Wang, W. Hu, X. Zhou, N. Guo, H. Huang, S. Sun, H. Shen, T. Lin, M. Tang, L. Liao, A. Jiang, J. Sun, X. Meng, X. Chen, W. Lu, J. Chu, Ultrasensitive and broadband MoS_2 photodetector driven by ferroelectrics, Adv. Mater. 27 (2015) 6575–6581.

[5] R. Mas-Balleste, C. Gomez-Navarro, J. Gomez-Herrero, F. Zamora, 2D materials: to graphene and beyond, Nanoscale 3 (2011) 20–30.

[6] S.B. Desai, S.R. Madhvapathy, A.B. Sachid, J.P. Llinas, Q. Wang, G.H. Ahn, G. Pitner, M.J. Kim, J. Bokor, C. Hu, H.P. Wong, A. Javey, MoS_2 transistors with 1-nanometer gate lengths, Science 354 (2016) 99–102.

[7] B. Radisavljevic, A. Radenovic, J. Brivio, V. Giacometti, A. Kis, Single-layer MoS_2 transistors, Nat. Nanotechnol. 6 (2011) 147–150.

[8] W. Liu, J. Kang, D. Sarkar, Y. Khatami, D. Jena, K. Banerjee, Role of metal contacts in designing high-performance monolayer n-type WSe_2 field effect transistors, Nano Lett. 13 (2013) 1983–1990.

[9] Y. Ma, Y. Dai, M. Guo, C. Niu, J. Lu, B. Huang, Electronic and magnetic properties of perfect, vacancy-doped, and nonmetal adsorbed $MoSe_2$, $MoTe_2$ and WS_2 monolayers, Phys. Chem. Chem. Phys. 13 (2011) 15546–15553.

[10] C. Ruppert, O.B. Aslan, T.F. Heinz, Optical properties and band gap of single- and few-layer $MoTe_2$ crystals, Nano Lett. 14 (2014) 6231–6236.

[11] I.G. Lezama, A. Arora, A. Ubaldini, C. Barreteau, E. Giannini, M. Potemski, A.F. Morpurgo, Indirect-to-direct band gap crossover in few-layer $MoTe_2$, Nano Lett. 15 (2015) 2336–2342.

[12] W. Zhang, Z. Huang, W. Zhang, Y. Li, Two-dimensional semiconductors with possible high room temperature mobility, Nano Res. 7 (2014) 1731–1737.

[13] Y.F. Lin, Y. Xu, S.T. Wang, S.L. Li, M. Yamamoto, A. Aparecido-Ferreira, W. Li, H. Sun, S. Nakaharai, W.B. Jian, K. Ueno, K. Tsukagoshi, Ambipolar $MoTe_2$ transistors and their applications in logic circuits, Adv. Mater. 26 (2014) 3263–3269.

[14] S. Nakaharai, M. Yamamoto, K. Ueno, Y.F. Lin, S.L. Li, K. Tsukagoshi, Electrostatically reversible polarity of Ambipolar alpha-$MoTe_2$ transistors, ACS Nano 9 (2015) 5976–5983.

[15] N.R. Pradhan, D. Rhodes, S. Feng, Y. Xin, S. Memaran, B.H. Moon, H. Terrones, M. Terrones, L. Balicas, Field-effect transistors based on few-layered alpha-$MoTe_2$, ACS Nano 8 (2014) 5911–5920.

[16] I.G. Lezama, A. Ubaldini, M. Longobardi, E. Giannini, C. Renner, A.B. Kuzmenko, A.F. Morpurgo, Surface transport and band gap structure of exfoliated 2H-$MoTe_2$ crystals, 2D Materials 1 (2014) 021002.

[17] S. Fathipour, N. Ma, W.S. Hwang, V. Protasenko, S. Vishwanath, H.G. Xing, H. Xu, D. Jena, J. Appenzeller, A. Seabaugh, Exfoliated multilayer $MoTe_2$ field-effect transistors, Appl. Phys. Lett. 105 (2014) 192101.

[18] H. Liu, M. Si, S. Najmaei, A.T. Neal, Y. Du, P.M. Ajayan, J. Lou, P.D. Ye, Statistical study of deep submicron dual-gated field-effect transistors on monolayer chemical vapor deposition molybdenum disulfide films, Nano Lett. 13 (2013) 2640–2646.

[19] S. McDonnell, B. Brennan, A. Azcatl, N. Lu, H. Dong, C. Buie, J. Kim, C.L. Hinkle, M.J. Kim, R.M. Wallace, HfO_2 on MoS_2 by atomic layer deposition: adsorption mechanisms and thickness scalability, ACS Nano 7 (2013) 10354–10361.

[20] J. Yang, S. Kim, W. Choi, S.H. Park, Y. Jung, M.H. Cho, H. Kim, Improved growth behavior of atomic-layer-deposited high-k dielectrics on multilayer MoS_2 by oxygen plasma pretreatment, ACS Appl. Mater. Interfaces 5 (2013) 4739–4744.

[21] A. Azcatl, S. McDonnell, K.C. Santosh, X. Peng, H. Dong, X.Y. Qin, R. Addou, G.I. Mordi, N. Lu, J. Kim, M.J. Kim, K. Cho, R.M. Wallace, MoS_2 functionalization for ultra-thin atomic layer deposited dielectrics, Appl. Phys. Lett. 104 (2014) 111601.

[22] L. Cheng, X. Qin, A.T. Lucero, A. Azcatl, J. Huang, R.M. Wallace, K. Cho, J. Kim, Atomic layer deposition of a high-k dielectric on MoS_2 using trimethylaluminum and ozone, ACS Appl. Mater. Interfaces 6 (2014) 11834–11838.

[23] X. Zou, J. Wang, C.H. Chiu, Y. Wu, X. Xiao, C. Jiang, W.W. Wu, L. Mai, T. Chen, J. Li, J.C. Ho, L. Liao, Interface engineering for high-performance top-gated MoS_2 field-effect transistors, Adv. Mater. 26 (2014) 6255–6261.

[24] Y.-S. Lin, P.-H. Cheng, K.-W. Huang, H.-C. Lin, M.-J. Chen, Atomic layer deposition of sub-10 nm high-K gate dielectrics on top-gated MoS_2 transistors without surface functionalization, Appl. Surf. Sci. 443 (2018) 421–428.

[25] I. Kwak, J.H. Park, L. Grissom, B. Fruhberger, A. Kummel, Mechanism of low temperature ALD of Al_2O_3 on graphene terraces, ECS Trans. 75 (2016) 143–151.

[26] I. Kwak, M. Kavrik, J.H. Park, L. Grissom, B. Fruhberger, K.T. Wong, S. Kang, A.C. Kummel, Low interface trap density in scaled bilayer gate oxides on 2D materials via nanofog low temperature atomic layer deposition, Appl. Surf. Sci. 463 (2019) 758–766.

[27] Q. Qian, B. Li, M. Hua, Z. Zhang, F. Lan, Y. Xu, R. Yan, K.J. Chen, Improved gate dielectric deposition and enhanced electrical stability for single-layer MoS_2 MOSFET with an AlN interfacial layer, Sci. Rep. 6 (2016) 27676.

[28] A. Azcatl, S. Kc, X. Peng, N. Lu, S. McDonnell, X. Qin, F. de Dios, R. Addou, J. Kim, M.J. Kim, K. Cho, R.M. Wallace, HfO_2 on UV–O_3 exposed transition metal dichalcogenides: interfacial reactions study, 2D Materials 2 (2015) 014004.

[29] H.Y. Shih, W.H. Lee, W.C. Kao, Y.C. Chuang, R.M. Lin, H.C. Lin, M. Shiojiri, M.J. Chen, Low-temperature atomic layer epitaxy of AlN ultrathin films by layer-by-layer, in-situ atomic layer annealing, Sci. Rep. 7 (2017) 39717.

[30] G. Lee, B. Lee, J. Kim, K. Cho, Ozone adsorption on graphene: ab initio study and experimental validation, J. Phys. Chem. C 113 (2009) 14225–14229.

[31] H. Liu, K. Xu, X.J. Zhang, P.D. Ye, The integration of high-k dielectric on two-dimensional crystals by atomic layer deposition, Appl. Phys. Lett. 100 (2012) 152115.

[32] Y. Kim, J.G. Song, Y.J. Park, G.H. Ryu, S.J. Lee, J.S. Kim, P.J. Jeon, C.W. Lee, W.J. Woo, T. Choi, H. Jung, H.B. Lee, J.M. Myoung, S. Im, Z. Lee, J.H. Ahn, J. Park, H. Kim, Self-limiting layer synthesis of transition metal dichalcogenides, Sci. Rep. 6 (2016) 18754.

[33] L.A. Riley, A.S. Cavanagh, S.M. George, Y.S. Jung, Y. Yan, S.H. Lee, A.C. Dillon, Conformal surface coatings to enable high volume expansion Li-ion anode materials, Chemphyschem 11 (2010) 2124–2130.

[34] C.-W. Chu, S.-H. Li, C.-W. Chen, V. Shrotriya, Y. Yang, High-performance organic thin-film transistors with metal oxide/metal bilayer electrode, Appl. Phys. Lett. 87 (2005) 193508.

[35] S. Guo, Z. Zhu, X. Hu, W. Zhou, X. Song, S. Zhang, K. Zhang, H. Zeng, Ultrathin tellurium dioxide: emerging direct bandgap semiconductor with high-mobility transport anisotropy, Nanoscale 10 (2018) 8397–8403.

[36] K. Choi, Y.T. Lee, J.S. Kim, S.-W. Min, Y. Cho, A. Pezeshki, D.K. Hwang, S. Im, Non-lithographic fabrication of all-2D α-$MoTe_2$ dual gate transistors, Adv. Funct. Mater. 26 (2016) 3146–3153.

[37] G. Eda, H. Yamaguchi, D. Voiry, T. Fujita, M. Chen, M. Chhowalla, Photoluminescence from chemically exfoliated MoS_2, Nano Lett. 11 (2011) 5111–5116.

[38] N.M.D. Brown, N. Cui, A. McKinley, An XPS study of the surface modification of natural MoS_2 following treatment in an RF-oxygen plasma, Appl. Surf. Sci. 134 (1998) 11–21.

[39] A. Azcatl, X. Qin, A. Prakash, C. Zhang, L. Cheng, Q. Wang, N. Lu, M.J. Kim, J. Kim, K. Cho, R. Addou, C.L. Hinkle, J. Appenzeller, R.M. Wallace, Covalent nitrogen doping and compressive strain in MoS_2 by remote N_2 plasma exposure, Nano Lett. 16 (2016) 5437–5443.

[40] M.B. Kanoun, S. Goumri-Said, M. Jaouen, Structure and mechanical stability of molybdenum nitrides: a first-principles study, Phys. Rev. B 76 (2007).

[41] I. Jauberteau, A. Bessaudou, R. Mayet, J. Cornette, J. Jauberteau, P. Carles, T. Merle-Méjean, Molybdenum nitride films: crystal structures, synthesis, mechanical, electrical and some other properties, Coatings 5 (2015) 656–687.

[42] C. Rice, R.J. Young, R. Zan, U. Bangert, D. Wolverson, T. Georgiou, R. Jalil, K.S. Novoselov, Raman-scattering measurements and first-principles calculations of strain-induced phonon shifts in monolayer MoS_2, Phys. Rev. B 87 (2013).

[43] S. Najmaei, Z. Liu, P.M. Ajayan, J. Lou, Thermal effects on the characteristic Raman spectrum of molybdenum disulfide (MoS_2) of varying thicknesses, Appl. Phys. Lett. 100 (2012) 013106.

[44] Y. Qi, P.G. Naumov, M.N. Ali, C.R. Rajamathi, W. Schnelle, O. Barkalov, M. Hanfland, S.C. Wu, C. Shekhar, Y. Sun, V. Suss, M. Schmidt, U. Schwarz, E. Pippel, P. Werner, R. Hillebrand, T. Forster, E. Kampert, S. Parkin, R.J. Cava, C. Felser, B. Yan, S.A. Medvedev, Superconductivity in Weyl semimetal candidate $MoTe_2$, Nat. Commun. 7 (2016) 11038.

[45] M. Yamamoto, S.T. Wang, M. Ni, Y.F. Lin, S.L. Li, S. Aikawa, W.B. Jian, K. Ueno, K. Wakabayashi, K. Tsukagoshi, Strong enhancement of Raman scattering from a bulk-inactive vibrational mode in few-layer $MoTe_2$, ACS Nano 8 (2014) 3895–3903.